J. Anat. (1995) 187, pp. 369–378, with 3 figures Printed in Great Britain

Patterns of morphological variation within myelin internodes of normal peripheral nerve: quantitative analysis by confocal microscopy

RHONDA J. REYNOLDS AND JOHN W. HEATH

The Neuroscience Group, University of Newcastle, New South Wales, Australia

(*Accepted 7 March 1995*)

ABSTRACT

Knowledge of variations in the morphology of normal myelinated peripheral nerve fibres is fundamental to subsequent interpretation of neuropathology. It would be advantageous for structural analysis of normal variations to be based on entire myelin internodes, but acquisition of such data via the classic approach of nerve fibre teasing has been hindered by limitations in optical resolution and specimen preparation. This study addressed these limitations through a new confocal imaging method which permits detailed visualisation of individual myelinated fibres in intact peripheral nerve trunks, and quantitated previously unrecognised patterns of morphological variation within normal internodes. The study focused particularly on Schmidt–Lanterman incisures, the narrow cytoplasmic channels which traverse normal compact myelin and provide foci for disruption of the compact sheath in a number of peripheral neuropathies. Analysis was based on confocal fluorescence images of multiple sequential internodes, traced within posterior tibial nerve trunks of adult male Sprague–Dawley rats. The strength of relationships between internodal size variables (length, fibre diameter, myelin sheath thickness) and total number of incisures per internode were documented. Each internode was divided into 4 regions of equivalent length (regions 1–4), and variations in the distribution of incisures and Schwann cell nuclear location were evaluated. Regional variations were consistent, irrespective of differences in fibre diameter, myelin sheath thickness, and internodal length. Expressed in terms of proximodistal orientation, there was a unimodal distribution of incisures within internodes of this fibre population (diameter range 5–9 μm), with region 3 containing the highest number of incisures and region 4 the lowest ($P < 0.05$). The Schwann cell nucleus was located more frequently in region 3 than in region 2 ($P < 0.01$). Contrary to previous reports, an incisure was found in close association with the nucleus in at least 50% of internodes. Documentation of frequent incisure–nuclear association and consistent patterns of variation within internodes extends knowledge of the microanatomy of normal peripheral nerve, and may provide insight into the functional role of incisures. Demonstration of such patterns in normal nerve may contribute to the understanding of pathological change, for example progression of ovoid formation from midinternodal regions during wallerian degeneration.

Key words: Rat; myelin sheath; Schmidt–Lanterman incisures; Schwann cells.

INTRODUCTION

Reliability of assessment of pathological change in myelinated peripheral nerve fibres depends on prior acquisition of appropriate control data for species, age, nerve, and level of nerve (Dyck et al. 1993). Analysis along entire internodes is potentially valuable in making such assessments, and traditionally has been based on teased fibres (Lubinska, 1977, 1982; Ghabriel & Allt, 1979*a*, 1980*a*; Ohi et al. 1985; Gabreëls-Festen et al. 1990; Sobue et al. 1992). However, acquisition of adequately detailed data for entire internodes (whether normal or pathological) has been hindered by artefacts frequently associated with nerve fibre teasing and sectioning (Ghabriel & Allt, 1980*a*; Dyck et al. 1993) and by the limited resolving power of conventional light microscopy (Webster, 1965). The advent of confocal microscopy

Correspondence to Ms Rhonda J. Reynolds, Medical Sciences Building (Room 509), Faculty of Medicine and Health Sciences, University of Newcastle, Callaghan, New South Wales 2308, Australia.

has provided a powerful new tool for investigating the nervous system (Murray, 1992). The enhanced resolution and increased depth of field provided by confocal microscopy now permits detailed imaging of individual myelinated fibres positioned within intact peripheral nerve trunks (Reynolds et al. 1994*b*). Utilising optical sectioning to trace individual fibres as they course through the trunk, it is possible to acquire detailed images of multiple consecutive internodes, including the form of the Schmidt–Lanterman incisures and position of the Schwann cell nuclei. The computer-assisted data storage and retrieval capacities of the confocal system enable reconstruction of entire internodes in longitudinal section. Notably, the method avoids disruption of adjacent cellular and extracellular relationships, now recognised as potentially significant in the development of nerve pathology and in subsequent regeneration (Burge, 1987; Seckel, 1990; Dyck et al. 1993; Griffin & Hoffman, 1993).

Numerous investigations of normal and pathological peripheral nerve have focused on the Schmidt–Lanterman incisures, yet their precise role has not been determined. Incisures represent channels of Schwann cell cytoplasm traversing the compact myelin spiral (Peters et al. 1991). The positive relationship between incisure frequency and myelin sheath thickness is well documented for normal nerve (Landon & Hall, 1976; Sunderland, 1978; Thomas et al. 1993), and several functions have been suggested. These include metabolic maintenance of the myelin sheath, transport of metabolites through the sheath to the axon, a mechanism providing for longitudinal growth of myelin segments, and contribution to peristaltic movement of axoplasm (reviewed by Ghabriel & Allt, 1981; Thomas et al. 1993). In addition, the functional importance of incisures has been inferred from studies of developing and pathological peripheral nerve (Ghabriel & Allt, 1981; Small et al. 1987). Incisures increase in numbers with increasing fibre diameter in developing (Hiscoe, 1947) and regenerating nerve (Ghabriel & Allt, 1980*a*, *b*). Incisures have long been known to provide foci for segmentation of the myelin sheath into ovoids during wallerian degeneration (Cajal, 1928; Webster, 1965; Williams & Hall, 1971; Ghabriel & Allt, 1979*a*, *b*). Incisures have also been identified as sites of early change in experimental models for human demyelinating disorders such as the intraneural injection of serum from experimental allergic neuritis (Saida et al. 1978) and acute disseminated encephalomyelitis (Saida et al. 1979). More recently a set of characteristic changes, specifically at incisures, has been noted in a variety of human peripheral neuropathies including HMSN I–III, Friedreich's ataxia and metachromatic leukodystrophy (Schröder & Himmelmann, 1992).

Despite recognition of the importance of Schmidt–Lanterman incisures there is little published information regarding their spatial distribution along individual internodes of normal nerve. Compared with the remainder of the internode, a lower frequency of incisures has been reported in paranodal and nuclear/paranuclear regions of the sciatic nerve in guinea pig (Webster, 1965) and rat (Ghabriel & Allt, 1980*a*, 1981). However, these reports were limited to incisure counts based on 'half-internodes' (i.e. one paranode to nucleus; Webster, 1965) or were qualitative only (Ghabriel & Allt, 1980*a*, 1981). Moreover, use of the Schwann cell nuclear position alone is likely to be an inaccurate means of delineating half-internodes, since the nucleus is often displaced away from the midpoint of the internode (Landon & Hall, 1976). In rat phrenic nerve, this displacement is more frequently towards the distal node (Bremner & Smart, 1965). These observations emphasise again the need for quantitative data documenting the distribution of incisures along *entire* internodes.

Against this background, this study aimed to apply confocal imaging as a means of assessing regional variations in normal internodal morphology, and was based on the posterior tibial nerve of sham control and unoperated control rats. A brief report of this work has been presented (Reynolds et al. 1994*a*).

MATERIALS AND METHODS

Animals

Eleven male Sprague–Dawley rats aged 13–18 wk (body weight 400–600 g) were used. This study was conducted in 2 stages. The initial analysis was undertaken on posterior tibial nerves from the left side (sham controls; see below) of 8 animals used in a companion study of wallerian degeneration. Three additional rats were then subjected to sham surgery on the left side but remained completely unoperated on the right. The left and right posterior tibial nerves of these 3 animals were compared to determine whether differences detected in the initial study might be attributable to sham surgery. Food and water were available ad libitum.

Surgical procedures (sham controls)

Surgical anaesthesia was induced and maintained with halothane in oxygen (4 and 2.5% respectively).

Table 1. *Numbers of internodes imaged: posterior tibial nerve*

Animals	Number of internodes	
	Left nerve	Right nerve
Sham controls (n = 8)	94	—
Sham controls vs unoperated controls (n = 3)	52	54

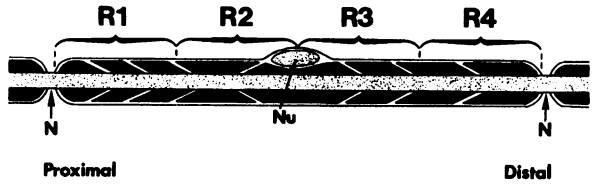

Fig. 1. Schematic representation of an internode showing its division into 4 regions of equivalent length. (< >), Schmidt–Lanterman incisures; R, region; N, node of Ranvier; Nu, Schwann cell nucleus.

Analgesia (buprenorphine HCl: 0.1 mg/kg s.c.) was administered immediately following induction of anaesthesia and at 8–12 hourly intervals thereafter. The right and left sciatic nerves were exposed midthigh, and approximately 0.5 cm of the nerve trunk mobilised by gentle dissection to free the epineurium from surrounding connective tissue. The overlying muscles and skin were sutured (5–0 Prolene propylene sutures) immediately on the left side (i.e. sham surgery) and following complete transection of the nerve trunk on the right. Transection of the right sciatic nerve is noted here to fulfil ethics reporting requirements, but data from these transected nerves are not the subject of this report. Animals were caged separately following surgery.

Perfusion fixation and tissue preparation

For killing, surgical anaesthesia was induced, initially with 4% halothane in oxygen, followed by an injection of pentobarbitone sodium (Nembutal; 90 mg/kg i.p.). Animals were perfused systemically (Furness et al. 1978) with 1% sodium nitrite containing heparin, followed by 5% glutaraldehyde (Electron Microscopy Sciences, Fort Washington, PA) in 0.1 M sodium cacodylate buffer at pH 7.4. Nerve trunks were removed and desheathed carefully under a dissecting microscope, stored overnight at 4 °C in the fixative solution used for perfusion and thereafter in the buffer solution alone. After a minimum storage period of at least 1 wk, whole posterior tibial nerve trunks were placed between 2 coverslips (Mediglass, thickness 0.085–0.13 mm) using the buffer solution as mountant (Reynolds et al. 1994*b*).

Fibre selection, confocal imaging and regional definitions

A total of 210 complete internodes was imaged, representing multiple sequences along 22 individual fibres (Table 1). Fibres were selected only if at least 7 sequential internodes could be imaged, in order to ensure comparability of these normal data in a future analysis of transected fibres. A second aspect influencing selection was that depth of imaging limitations associated with confocal microscopy (Reynolds et al. 1994*b*) restricted sampling to fibres coursing the perimeter of the nerve trunks, to a depth of 25–30 μm approximately.

Nerve trunks were examined using a Bio-Rad MRC-600 confocal laser scanning imaging system linked to a Zeiss Axiovert 10 inverted microscope equipped with a ×40, NA 1.3 Plan-Neofluar oil objective lens (Zeiss, West Germany). The excitation source was an argon ion laser (Ion Laser Technology, Salt Lake City, Utah, USA) attenuated using 1% transmission and a Bio-Rad BHS filter set (excitation wavelength 488 nm; dichroic mirror 510 nm; barrier filter 515 nm). Full frame 768 × 512 pixel images were collected and stored using a Canon MO-5001S high-capacity optical data storage system (Canon Inc., Japan) linked to a 386 IBM-compatible microcomputer. The range of intensities per pixel was 0–255. All images were collected with the zoom facility set at 2.0. Aperture, gain levels and Kalman averaging were adjusted to optimise the imaging of each individual fibre. Individual images collected along the entire extent of each internode were printed at the same final magnification (9 mm = 10 μm) using a CP100E colour video copy processor (Mitsubishi Electric Corporation, Japan).

Maintaining their proximodistal orientation, photomontages of each internode were prepared and divided into 4 regions (R) equivalent in length (R1 = proximal; R4 = distal; see Fig. 1).

Quantitation

(1) *Internode length* was measured (from midpoints of the proximal and distal nodes of Ranvier). (2) *Fibre diameter* was recorded at 2 points spaced equally between every pair of adjacent incisures along each internode, as well as at 1 point between each node and the closest incisure. Wherever possible, the measurements avoided regions of obvious outpocketing of the

Table 2. *Sham control internodes**

Size parameter	Class 1 (5–7 μm) (n = 43) Mean (μm)	S.E.M. (μm)	Class 2 (> 7–9 μm) (n = 51) Mean (μm)	S.E.M. (μm)	t value	2-tailed probability
Internode length	814.86	22.56	949.89	17.82	−4.76	***
Fibre diameter	6.45	0.06	7.84	0.06	−15.81	***
Myelin sheath thickness	1.69	0.03	2.01	0.03	−7.49	***
Interincisural distance	66.74	1.49	53.40	1.03	7.51	***
End segments						
proximal	75.87	3.81	6.67	4.03	1.64	ns
distal	76.90	5.35	64.92	3.47	1.93	ns

* Mean, S.E.M. and results of tests of difference between size parameters describing two classes of myelinated fibres.
***, $P < 0.001$; ns, not significant ($P > 0.05$).

internodal sheath. From these measurements, mean fibre diameters were calculated. (3) The lengths of *proximal and distal 'end segments'* (Ghabriel & Allt, 1979*a*) were measured (from midpoint of node to midpoint of the nearest incisure). (4) Mean *inter-incisural distance* was calculated for each internode, according to the formula: internode length/(number of incisures + 1). (5) *Internodal myelin sheath thickness* was measured at 1 point along each internode, avoiding sites of tangential section through the compact sheath. (6) The *number of Schmidt–Lanterman incisures* was recorded for each internodal region (see Fig. 1) and each internode. Where an incisure was found at a regional boundary, its position was assigned according to the location of its narrowest diameter (i.e. the region at which the angled incisural cleft abuts the axon). (7) Where possible the *regional location of the Schwann cell nucleus* was recorded. In the few instances where the nucleus lay at a regional boundary, its position was assigned according to the location of the greater part of its volume. (8) The occurrence of an *incisure in association with the Schwann cell nucleus* was recorded, where an incisure was found within the length of myelin sheath indented by the Schwann cell nucleus.

Statistical evaluation

Analyses were performed using the SPSS statistical package (SPSS Reference Guide, 1990). The primary aim of this investigation was to examine regional variations in the distribution of incisures. Two sets of data were obtained (see Table 1; also *Animals*, this Section). Internodes from the first data set (sham control nerves only) were classified into groups according to 2 ranges of fibre diameter (class 1: 5–7 μm versus class 2: > 7–9 μm) to test for between-group differences. Because this initial study showed there were no variations in incisure distribution due to differing fibre diameter, internodes from the second data set were not classified according to diameter. Thus between-group differences for the second study refer to comparisons between sham controls and unoperated controls.

(1) Two-way ANOVA was performed to evaluate the data on the regional distribution of incisures. For each data set these analyses permitted consideration of 2 main effects (differences between groups in mean numbers of incisures for the entire internode; and differences within groups in mean numbers of incisures per region, without taking the between-group differences into account). These analyses also permitted consideration of an interaction effect (i.e. whether mean numbers of incisures for the 2 groups comprising each sample varied in parallel across the 4 regions). Between-group effects were assessed using a standard univariate approach. Interactions and within-group (i.e. region) effects were tested via a multivariate approach, in order to avoid potential violations of assumptions of ANOVA that can result from combining unequal between-group sample sizes and within-group (repeated) measures in a 2-way factorial design (Bray & Maxwell, 1986). Significant within-group (region) effects were followed up with specific comparisons (orthogonal polynomials) to determine whether a significant trend (order) of incisure distribution was evident along the internode. The latter results were evaluated using Scheffé's contrast procedure (Berenson et al. 1983).

(2) To establish whether individual parameters of fibre size (see Tables 2, 3) were different between groups of fibres t tests were performed. Between-group differences in mean internode length, fibre diameter, myelin sheath thickness, interincisural dis-

Table 3. *Comparison of sham control and unoperated control internodes*‡

Size parameter	Sham control (n = 52) Mean (μm)	S.E.M. (μm)	Unoperated control (n = 54) Mean (μm)	S.E.M. (μm)	t value	2-tailed probability
Internode length	948.72	27.61	808.43	21.33	4.04	***
Fibre diameter	7.09	0.07	7.02	0.09	0.52	ns
Myelin sheath thickness	1.78	0.02	1.77	0.03	0.10	ns
Interincisural distance	55.11	1.59	49.27	1.66	2.55	*
End segments						
proximal	67.59	4.21	62.90	3.06	0.91	ns
distal	62.54	3.29	59.36	2.84	0.73	ns

‡ Mean, S.E.M. and results of tests of difference between size parameters.
***, $P < 0.001$; *, $P < 0.05$; ; ns, not significant ($P > 0.05$).

tance, and proximal and distal end segments were analysed using independent-sample t tests. Differences between mean lengths of proximal and distal end segments within the same (groups of) internodes were assessed using paired-sample t tests.

(3) Pearson product–moment correlations were used to determine the degree of relationships between internode length, fibre diameter, myelin sheath thickness and total numbers of incisures per internode.

(4) The frequency data on regional locations of Schwann cell nuclei were analysed using χ^2 tests.

RESULTS

Sham control nerves

Morphometry and internode reconstruction. The high degree of resolution provided by the optical sectioning capability of the confocal microscope facilitated measurement of internode length, interincisural distance, fibre diameter, myelin sheath thickness and the length of end segments. In particular, preparation of a photomontage of each internode enabled its division into 4 regions of equivalent length (R1–R4; Fig. 2) as the basis for evaluation of proximodistal variations. Table 2 shows mean values and S.E.M. for 6 size parameters describing morphological features of the 94 internodes, tabulated for the 2 ranges of fibre diameter (class 1: 5.0–7.0 μm; class 2: > 7.0–9.0 μm). As anticipated from the literature (Hiscoe, 1947; Sunderland, 1978), independent t tests (Table 2) indicated that the internode length, myelin sheath thickness and (by definition) fibre diameter of class 1 fibres were significantly less than those of class 2, while the mean interincisural distance was significantly larger ($P < 0.001$). However, a novel finding was that there were no differences between these 2 fibre classes in the lengths of either proximal or distal end segments ($P > 0.05$).

Schwann cell nucleus location. In 62% of the internodes examined the location of the Schwann cell nucleus was readily determined, either by its indentation of the compact sheath and/or by fluorescence emanating from the nucleoli (Fig. 2). The nucleus was located significantly more often in R3 (71%) than in R2 (29%) [$\chi^2(1) = 10.59$; $P < 0.01$]. Similar directional variation in nuclear position was evident along sequential internodes of individual fibres as well as in the general fibre population. Notably, a Schmidt–Lanterman incisure was found in association with the nucleus (Fig. 2) in 51% of internodes. The mean distance of displacement (midpoint of internode to midpoint of nucleus) was 23 μm in distally displaced nuclei and 13 μm in those displaced in the proximal direction. The greatest distances of displacement observed were approximately 100 μm (distally) and 30 μm (proximally).

Distribution of incisures. The regional distribution of incisures (means and S.E.M.) are plotted in Figure 3, for the 2 fibre classes. A 2 × 4 (class × region) ANOVA, with repeated measures over region, indicated significant main effects of class ($F[1,92] = 79.5$; $P < 0.001$) and region ($F[3,90] = 21.1$; $P < 0.001$). The mean number of incisures was significantly higher in class 2 than class 1 fibres (17.1 vs 11.4). Scheffé follow-up comparisons of regional means revealed a significant quadratic component of trend ($F[1,92] = 56.6$; $P < 0.001$) with R3 having the highest mean number of incisures. As indicated in Figure 3, there was a gradual increase in the mean number of incisures from R1 to R3 while the largest decrease occurred between R3 and R4. The interaction effect was not significant ($P > 0.05$) indicating no

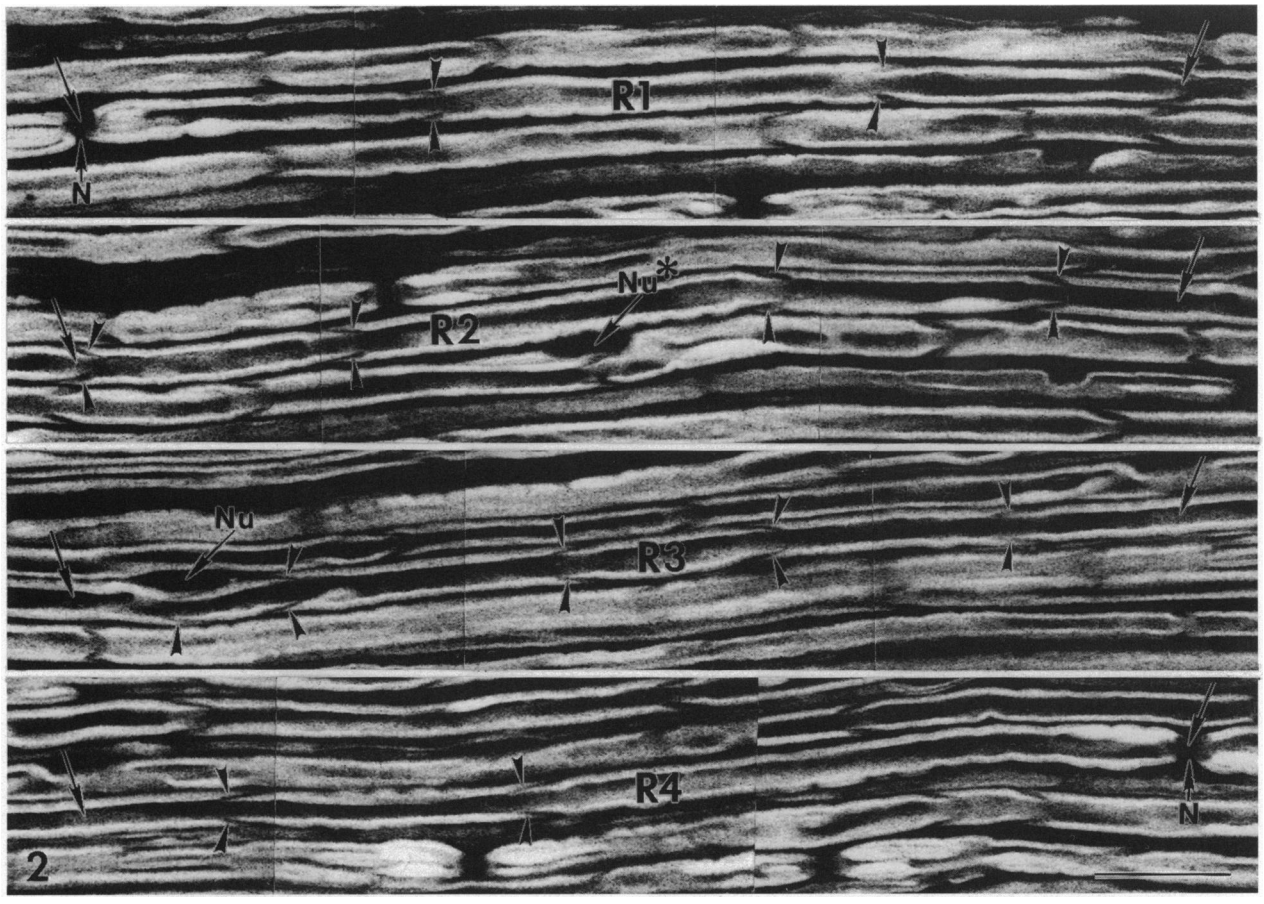

Fig. 2. Confocal imaging of an entire internode (length: 817 μm; mean diameter: 7.2 μm) with the 4 regions indicated by R1 (proximal)–R4 (distal), and delineated by arrows. Continuity is from the right arrow of one panel to the left arrow of the panel below. In this internode the nucleus (Nu) is in region 3 and is associated with an incisure. Incisure–nuclear association (Nu*) is also present in a neighbouring internode (panel 2). Arrowheads, Schmidt–Lanterman incisures; N, nodes of Ranvier. Bar, 25 μm.

differences between the 2 fibre classes in the trend of distribution of incisures along internodes.

Length of end segments. Paired t tests revealed no differences ($P > 0.05$) between the proximal and distal end segments within either class 1 or class 2 fibres, indicating an absence of any consistent proximodistal gradient of variation within the internode with respect to the distance between each node and its nearest incisure.

Comparison of sham control and unoperated control nerves

Independent t tests (Table 3) indicated that there were no differences between mean fibre diameter, myelin sheath thickness, and lengths of proximal and distal end segments of sham control and unoperated control internodes ($P > 0.05$). In addition, paired t tests showed no differences between the length of proximal and distal end segments within internodes ($P > 0.05$). However, mean internodal length and interincisural distance were significantly greater in the sham-operated nerves than in the unoperated controls ($P < 0.001$ and $P < 0.05$, respectively; Table 3). A 2×4 (nerve type × region) ANOVA, with repeated measures over region, also revealed that while there were no differences ($P > 0.05$) between the mean number of incisures (16.7 vs 16.1, respectively) in sham control and unoperated control internodes, there was a significant main effect of region ($F[3,102] = 21.8$; $P < 0.001$). Scheffé follow-up comparisons revealed a significant quadratic component of trend in the distribution of incisures ($F[1,104] = 57.0$; $P < 0.001$). This distribution was of the same order (R3 > R2 > R1 > R4) as the internodes examined in the initial investigation using sham-operated nerves only. There was no interaction effect ($P > 0.05$), indicating no difference between sham-operated and unoperated nerves with respect to the regional distribution of incisures. χ^2 analyses showed a significant trend of distal location (i.e. region 3) of the Schwann cell nucleus (73% of those identified – $\chi^2(1) = 16.9$; $P < 0.001$), but no difference ($P > 0.05$) between sham control and unoperated

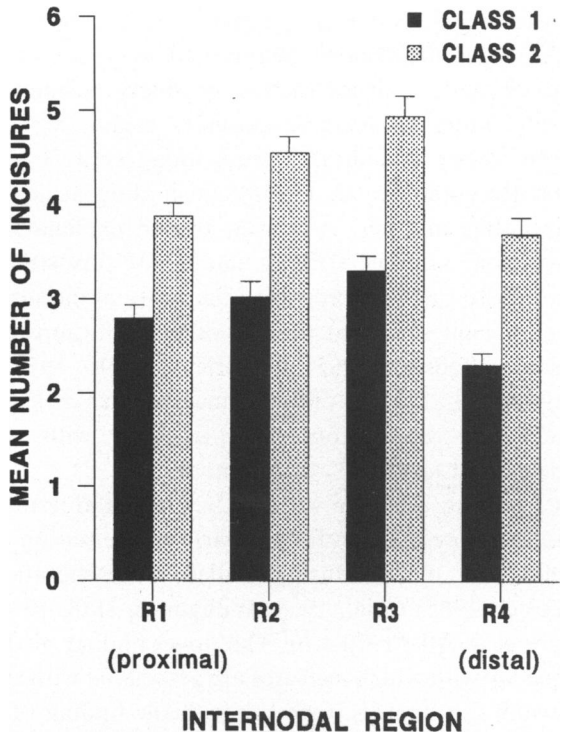

Fig. 3. Graphic representation of the regional distribution of incisures within internodes, showing means and S.E.M. for class 1 (5–7 μm) and class 2 (> 7–9 μm) fibres. R, region.

control internodes. Taken together, these quantitative data indicate that there were no differences between sham control and unoperated control internodes with respect to regional variations in incisure distribution and nuclear location. Although the mean length of internodes comprising the sham control sample was greater than that of unoperated controls, this difference was not considered to affect the results obtained. This inference was based on the results from the initial sham control investigation, in which the internode lengths of the two fibre classes also differed. If it were the case that differences in internode length affected incisure distribution and Schwann cell nuclear location, this effect should have been apparent in that first data set. This was not the case. Thus the documented regional variations in internodal morphology appear to be a feature of normal nerve, and not attributable to sham surgery per se.

Correlations between internodal size parameters

Table 4 shows results of correlations performed between total numbers of incisures per internode, fibre diameter, myelin sheath thickness and internode length. The results are tabulated for data from the two studies. Thus the confocal approach enabled us to present quantitative data documenting the degree of inter-relationships between all these features of the myelin sheath, simultaneously. As anticipated from the literature, the data indicate positive correlations between all parameters; all but one of the 36 correlations were significant (Table 4).

DISCUSSION

Combining confocal imaging of individual myelinated fibres in whole peripheral nerve trunks (Reynolds et al. 1994*b*) with quantitation this study has, for the first time, demonstrated consistent patterns of variation in the distribution of Schmidt–Lanterman incisures along entire internodes of normal fibres. Expressed in terms of a proximal-to-distal orientation and 4 regions of equivalent length defined along the

Table 4. *Sham control and sham control vs unoperated control internodes*

		Sham control internodes			SC vs UC internodes		
Variables correlated		Total (n = 94)	Class 1 (n = 43)	Class 2 (n = 51)	Total (n = 106)	SC (n = 52)	UC (n = 54)
Number of incisures	Internode length	0.78**	0.75**	0.68**	0.52**	0.63**	0.41**
	Fibre diameter	0.76**	0.44**	0.35*	0.53**	0.72**	0.39**
	MST	0.72**	0.42**	0.50**	0.68**	0.54**	0.81**
Internode length	Fibre diameter	0.63**	0.51**	0.46**	0.32**	0.45**	0.22 ns
	MST	0.64**	0.43**	0.53**	0.41**	0.46**	0.45**
Fibre diameter	MST	0.77**	0.46**	0.58**	0.48**	0.58**	0.43**

Correlation matrix showing r values calculated for relationships between number of incisures per internode, diameter, myelin sheath thickness and internode length. r values from sham-control nerves of both groups of animals were compared using Fisher's test (Howell, 1987). Five of the 6 relationships were not different ($P > 0.05$). There was a significant difference between the 2 groups in the strength of relationship between fibre diameter and myelin sheath thickness ($P < 0.05$), but this effect is unlikely to interfere with interpretation of the main results reported elsewhere in this paper. Taken as a whole, these results strongly support the similarity of the sham-control nerve fibre populations analysed.

SC, sham controls; UC, unoperated controls; MST, myelin sheath thickness; **, $P < 0.01$; *, $P < 0.05$; ns, not significant ($P > 0.05$).

internode, incisures displayed a unimodal distribution, with the third region containing the highest number of incisures and the fourth region the lowest. In addition, a substantial majority of Schwann cell nuclei were displaced distal to the internodal midpoint. The latter data appear to be the first in support of an earlier brief report on rat phrenic nerve (Bremner & Smart, 1965), findings hitherto discounted due to the absence of corroborating evidence (Landon & Hall, 1976). The patterns of variation in incisure distribution and nuclear location documented in this study complement other previously recognised variations along normal nerve fibres, such as changes in myelin sheath thickness, axon calibre, and the size of incisures (Friede & Samorajski, 1968; Fraher, 1973; Sunderland, 1978). In addition, the findings may be relevant to accurate assessment of pathological change in myelin internodes.

Results from the initial study using sham control nerves demonstrated a consistent pattern of Schmidt–Lanterman incisures within internodes, even though the data were analysed in terms of 2 separate ranges of fibre diameter. Subsequent statistical tests revealed that the internode length and myelin sheath thickness of these two fibre classes (defined in terms of diameter) were also from separate ranges. When nerves from a second group of sham-operated rats were compared with those from the contralateral unoperated nerves, a similar distribution of incisures within internodes was found. This result emerged in the second group even though the mean internode length was actually different in the fibre samples from the right and left sides. Thus there was a consistent pattern of intercalation of incisures along internodes, irrespective of the internodal length, the myelin sheath thickness or the fibre diameter.

The finding of relatively more Schmidt–Lanterman incisures in the 2 midregions (R2, R3) of the internode departs from the quantitative data of Webster (1965), the observations of Ghabriel & Allt (1979*a*), and the view that incisures tend not to be present in perinuclear regions (reviewed by Thomas et al. 1993). There are several explanations for these differences. First, the quantitative data of Webster (1965) were obtained from half-internodes. Since the proximodistal fibre orientation was not retained in Webster's study, asymmetric variations of incisure distribution within the half-internodes may have tended to cancel out. Secondly, the half-internodes analysed in the same study were defined as 'node of Ranvier to Schwann cell nucleus'. Since location of the Schwann cell nucleus is usually not at the true internodal midpoint (this paper; see also comments of Webster, 1965; Bremner & Smart, 1965; Landon & Hall, 1976), the regions quantitated may not have been absolute half-internodes in many instances. Thirdly, confocal imaging provides clearer visualisation of key structural features along entire internodes (Reynolds et al. 1994*b*), facilitating accurate quantitative analysis. A fourth, related explanation arises from another striking finding of this study. Contrary to previous reports of the rarity of incisures in the myelin sheath at the site of the Schwann cell nucleus (Webster, 1965; Ghabriel & Allt, 1979*a*; Gould et al. 1995), confocal imaging was able to demonstrate association of an incisure with the nucleus in at least 50% of internodes.

It has long been known that Schmidt–Lanterman incisures represent foci for the early segmentation of myelin into ovoids during wallerian degeneration (Webster, 1965; Cajal, 1968; Williams & Hall, 1971; Ghabriel & Allt, 1979*a*, *b*). The novel finding of the frequency with which incisures are associated with the Schwann cell nucleus, together with the finding of a significantly greater number of incisures in the midregions of the internode, may explain the previously documented initial progression of ovoid formation from the midregion of the internode during wallerian degeneration (Lubinska, 1977). It remains to be ascertained whether the region of initial progression is determined by the position of the nucleus per se, or simply occurs at the region of greatest clustering of Schmidt–Lanterman incisures within that internode. If incisures continue to play a role in transport across the myelin sheath during wallerian degeneration, these data may also explain the recently reported translocation of A-1 antigen (a putative marker of experimental peripheral nerve injury) from nuclear regions to the membranes of myelin ovoids following axotomy (Azzarelli *et al.* 1993).

An additional insight provided by the confocal imaging approach was that variation in the direction of nuclear displacement was evident along sequential internodes of individual fibres as well as in the general fibre population. This indicates that the direction of displacement is probably not explained by a simple dichotomy of fibre types, for example motor vs sensory. Possibly the nucleus is mobile within a relatively broad region of the internode: it may be found at a paranode in short internodes (Heath, 1982). The functional significance of predominantly distal displacement remains to be determined.

Another novel finding was that there were no consistent differences between the lengths of proximal and distal end segments *within* each group of

internodes. These results are surprising, given the long-known asymmetry of the proximal and distal paranodal bulbs associated with an individual node of Ranvier (Lubinska, 1954; Landon & Hall, 1976). In addition, the present study found no difference (i.e. in the length of end segments) *between* groups of internodes that were significantly different in other respects (e.g. in fibre diameter, internodal length, myelin sheath thickness). Also of note, the length of end segments was greater than the interincisural distance in all groups of fibres (see also Hiscoe, 1947; Gould et al. 1995). Taken together, these findings may provide indirect evidence for a role for incisures in the maintenance and metabolism of internodal myelin (Hiscoe, 1947; Ghabriel & Allt, 1980*a*). First, the paranodal sheath progressively diminishes in thickness as the compact myelin lamellae terminate in sequence to form the cytoplasmic pockets, and maintenance of this region may be less demanding metabolically than an equivalent length of internodal sheath. Secondly, the exceptionally high number of mitochondria in the paranodal Schwann cell cytoplasm (see Thomas et al. 1993) might partly support local myelin maintenance and reduce the need for paranodal incisures.

ACKNOWLEDGEMENTS

We thank Terry Lewin for advice on statistical evaluation and Peter Dunkley and Bruce Walmsley for constructive criticism of the manuscript. This work was funded by the National Multiple Sclerosis Society of Australia.

REFERENCES

AZZARELLI B, WOODBURN R, OLIVELLE S, KIMBRO S, SIAKOTOS A, TAYLOR M et al. (1993) The A-1 antigen: a novel marker in experimental peripheral nerve injury. *Journal of Comparative Neurology* **337**, 353–365.

BERENSON ML, LEVINE DM, GOLDSTEIN M (1983) *Intermediate Statistical Methods and Applications. A Computer Package Approach*. Englewood Cliffs, NJ: Prentice Hall.

BRAY JH, MAXWELL SE (1986) *Multivariate Analysis of Variance*. London: Sage.

BREMNER D, SMART I (1965) The position of Schwann cell nuclei in relation to the internodal mid-point of myelinated nerve fibres. *Journal of Anatomy* **99**, 194–195.

BURGE P (1987) Plastic and reconstructive surgery peripheral nerve injuries. *Hospital Update* **13**, 525–536.

CAJAL S, RAMON Y (1928) *Degeneration and Regeneration of the Nervous System*, vol. 1. New York: Hafner.

DYCK PJ, GIANNINI C, LAIS A (1993) Pathologic alterations of nerves. In *Peripheral Neuropathy*, 3rd edn, vol. 1 (ed. P. J. Dyck, P. K. Thomas, J. W. Griffin, P. A. Low & J. F. Poduslo), pp. 514–595. Philadelphia: W. B. Saunders.

FRAHER JP (1973) A quantitative study of anterior root fibres during early myelination. II. Longitudinal variation in sheath thickness and axon circumference. *Journal of Anatomy* **115**, 421–444.

FRIEDE RL, SAMORAJSKI T (1968) Myelin formation in the sciatic nerve of the rat. A quantitative electron microscopic, histochemical and radioautographic study. *Journal of Neuropathology and Experimental Neurology* **27**, 546–570.

FURNESS JB, HEATH JW, COSTA M (1978) Aqueous aldehyde (Faglu) methods for the fluorescence histochemical localization of catecholamines and for ultrastructural studies of central nervous tissue. *Histochemistry* **57**, 285–295.

GABREËLS-FESTEN AAWM, JOOSTEN EMG, GABREËLS FJM, STEGEMAN DF, VOS AJM, BUSCH HFM (1990) Congenital demyelinating motor and sensory neuropathy with focally folded myelin sheaths. *Brain* **113**, 1629–1643.

GHABRIEL MN, ALLT G (1979*a*) The role of Schmidt–Lanterman incisures in Wallerian degeneration. I. A quantitative teased fibre study. *Acta Neuropathologica (Berlin)* **48**, 83–93.

GHABRIEL MN, ALLT G (1979*b*). The role of Schmidt–Lanterman incisures in Wallerian degeneration. II. An electron microscopic study. *Acta Neuropathologica (Berlin)* **48**, 95–103.

GHABRIEL MN, ALLT G (1980*a*) Schmidt–Lanterman incisures. I. A quantitative teased fibre study of remyelinating peripheral nerve fibres. *Acta Neuropathologica (Berlin)* **52**, 85–95.

GHABRIEL MN, ALLT G (1980*b*) Schmidt–Lanterman incisures. II. A light and electron microscope study of remyelinating peripheral nerve fibres. *Acta Neuropathologica (Berlin)* **52**, 97–104.

GHABRIEL MN, ALLT G (1981) Incisures of Schmidt–Lanterman. *Progress in Neurobiology* **17**, 25–58.

GOULD RM, BYRD AL, BARBARESE E (1995) The number of Schmidt–Lanterman incisures is more than doubled in *shiverer* PNS myelin sheaths. *Journal of Neurocytology* **24**, 85–98.

GRIFFIN JW, HOFFMAN PN (1993) Degeneration and regeneration in the peripheral nervous system. In *Peripheral Neuropathy*, 3rd edn, vol. 1 (ed. P. J. Dyck, P. K. Thomas, J. W. Griffin, P. A. Low & J. F. Poduslo), pp. 361–376. Philadelphia: W. B. Saunders.

HEATH JW (1982) Double myelination of axons in the sympathetic nervous system. *Journal of Neurocytology* **11**, 249–262.

HISCOE HB (1947) Distribution of nodes and incisures in normal and regenerated nerve fibres. *Anatomical Record* **99**, 447–475.

HOWELL DC (1987) *Statistical Methods for Psychology*, 2nd edn, pp. 1–636. Boston: Duxbury Press.

LANDON DN, HALL S (1976) The myelinated nerve fibre. In *The Peripheral Nerve* (ed. D. N. Landon), pp. 1–105. New York: Chapman and Hall.

LUBINSKA L (1954) Form of myelinated nerve fibres. *Nature* **173**, 867–869.

LUBINSKA L (1977) Early course of Wallerian degeneration in myelinated fibres of the rat phrenic nerve. *Brain Research* **130**, 47–63.

LUBINSKA L (1982) Patterns of Wallerian degeneration of myelinated fibres in short and long peripheral stumps and in isolated segments of rat phrenic nerve. Interpretation of the role of axoplasmic flow of the trophic factor. *Brain Research* **233**, 227–240.

MURRAY JM (1992) Neuropathology in depth: the role of confocal microscopy. *Journal of Neuropathology and Experimental Neurology* **51**, 475–487.

OHI T, KYLE RA, DYCK PJ (1985) Axonal attenuation and secondary segmental demyelination in myeloma neuropathies. *Annals of Neurobiology* **17**, 255–261.

PETERS A, PALAY S, WEBSTER H DE F (1991) *The Fine Structure of the Nervous System: The Neurons and Supporting Cells*, 3rd edn. New York: Oxford University Press.

REYNOLDS RJ, LITTLE GJ, HEATH JW (1994*a*). Individual myelinated fibres traced through multiple consecutive internodes in whole PNS nerve trunks using confocal fluorescence microscopy: a new method for analysing regional variations in fibre

morphology. *Proceedings of the Peripheral Nerve Society, Saint Paul, Minnesota* 82 (Abstract).

REYNOLDS RJ, LITTLE GJ, LIN M, HEATH JW (1994*b*) Imaging myelinated nerve fibres by confocal fluorescence microscopy: individual fibres in whole nerve trunks traced through multiple consecutive internodes. *Journal of Neurocytology* **23**, 555–564.

SAIDA K, SAIDA T, BROWN MJ, SILBERBERG DH, ASBURY AK (1978) Antiserum-mediated demyelination in vivo: a sequential study using intraneural injection of experimental allergic neuritis serum. *Laboratory Investigation* **39**, 449–462.

SAIDA T, SAIDA K, BROWN MJ, SILBERBERG DH (1979) Peripheral nerve demyelination induced by intraneural injection of experimental allergic encephalomyelitis serum. *Journal of Neuropathology and Experimental Neurology* **38**, 498–518.

SCHRÖDER JM, HIMMELMANN F (1992) Fine structural evaluation of altered Schmidt–Lanterman incisures in human sural nerve biopsies. *Acta Neuropathologica (Berlin)* **83**, 120–133.

SECKEL BR (1990) Enhancement of peripheral nerve regeneration. *Muscle and Nerve* **13**, 785–800.

SMALL JR, GHABRIEL MN, ALLT G (1987) The development of Schmidt–Lanterman incisures: an electron microscope study. *Journal of Anatomy* **150**, 277–286.

SOBUE G, DOYU M, WATANABE M, HAYASHI F, MITSUMA T (1992) Extensive demyelinating changes in the peripheral nerves of Crow–Fukase syndrome: a pathological study of one autopsied case. *Acta Neuropathologica (Berlin)* **84**, 171–177.

SPSS REFERENCE GUIDE (1990). Chicago: SPSS inc.

SUNDERLAND S (1978) *Nerves and Nerve Injuries*, 2nd edn. London: Churchill Livingstone.

THOMAS PK, BERTHOLD CH, OCHOA J (1993) Microscopic anatomy of the peripheral nervous system. In *Peripheral Neuropathy*, 3rd edn, vol. 1 (ed. P. J. Dyck, P. K. Thomas, J. W. Griffin, P. A. Low & J. F. Poduslo), pp. 28–91. Philadelphia: W. B. Saunders.

WEBSTER H DE F (1965) The relationship between Schmidt–Lanterman incisures and myelin segmentation during Wallerian degeneration. *Annals of the New York Academy of Sciences* **122**, 29–38.

WILLIAMS PL, HALL SM (1971) Chronic Wallerian degeneration – an in vivo and ultrastructural study. *Journal of Anatomy* **109**, 487–503.